ECN › TNO innovation for life

Westerduinweg 3
1755 LE Petten
P.O. Box 15
1755 ZG Petten
The Netherlands

www.tno.nl

T +31 88 866 50 65

TNO report

TNO 2018 R11648

Baseline Mexico rotor CFD simulations with SU2 and OpenFOAM

Date	December 2018
Author(s)	K. Vimalakanthan, K. Boorsma
Copy no	
No. of copies	
Number of pages	37 (incl. appendices)
Number of appendices	
Sponsor	
Project name	
Project number	

Since April 1st ECN and TNO have joined forces.

Managementuittreksel

Titel	:	Baseline Mexico rotor CFD simulations with SU2 and OpenFOAM
Auteur(s)	:	K. Vimalakanthan, K. Boorsma
Datum	:	December 2018
Opdrachtnr.	:	
Rapportnr.	:	TNO 2018 R11648

Summary

Numerical results for the 4.5 meter diameter wind tunnel tested Mexico rotor have been successfully established with two in-house CFD solvers (SU2 and OpenFoam) using a constant but relatively coarse grid. Still the simulations heavily suffered from limited computation power, in particular for SU2 which could not be parallelised efficiently and hence had a much longer calculation time than OpenFoam. However, the flow field and the blade pressures are resolved better by SU2.

This work is part of an ongoing effort to establish a CFD tool for wind turbine modeling within ECN part of TNO, and the aim of this initial investigation is to assess the capability of in-house CFD tools by comparing these first results to the measurements from the (New) Mexico rotor database. It is important to note that one should not draw any conclusions based on the presented results and it only serves as a general comparison of the initial effort to establish numerical results from both solvers. A grid independent solution from both solvers is required to establish a tangible conclusion on the solvers. Nevertheless, based on this initial results to date, SU2's compressible solver appears to be a versatile tool for wind energy applications.

Contents

1 Introduction

Computational Fluid Dynamics (CFD) has become and important tool in wind turbine design and research. Also at ECN part of TNO there is an ongoing effort to establish CFD models to simulate wind turbine rotor aerodynamics. The aim of this investigation is to assess the capability of several in-house CFD tools. Thereto blade resolved 3D rotor simulations are compared using two open source CFD solvers: SU2 and OpenFOAM. SU2 is a compressible CFD code from Stanford University[4], and OpenFOAM solves the incompressible Navier-Stokes equations [5][6].

The New Mexico wind turbine validation cases [1] were chosen for this investigation. This experiment considers a fully instrumented three bladed 4.5 m diameter rotor tested in the large open jet facility of the German Dutch Wind Tunnels (DNW). The comparison of the results were carried out using the post processing methods as used in IEA Wind Task 29 Mexnext [2]. Three different operating scenarios in axial flow ranging from the turbulent wake state to the design point and separated flow conditions were considered. The presented results only serve as a general comparison of the initial effort to establish numerical results from both solvers. This report outlines these initial comparison to date, mainly focusing on the details of the simulation methods. First the CFD models including their set-up are described after which the results are presented and discussed.

2 CFD Model

This section details the geometry and CFD methods used to conduct the simulations. In this initial stage of the study a simpler geometry was used without considering the nacelle, tower or the tunnel walls. An axi-symetric rotor model considering only one blade passage is simulated based on the CAD data: BladeCore-B_Airfoil_11.igs (Figure 1a) from Technion. A pitch angle of -2.3° was applied to the blade as described in [2]. The actual hub, tower or the tunnels walls are not considered, instead a simple circular hub with rotor in uniform flow condition is modeled.

Three operational state of the Mexico rotor were simulated, these conditions are shown in Table 1.

Figure 1: Mexico blade and hub geometry with surface mesh

(a) Mexico blade and hub geometry   (b) Surface mesh
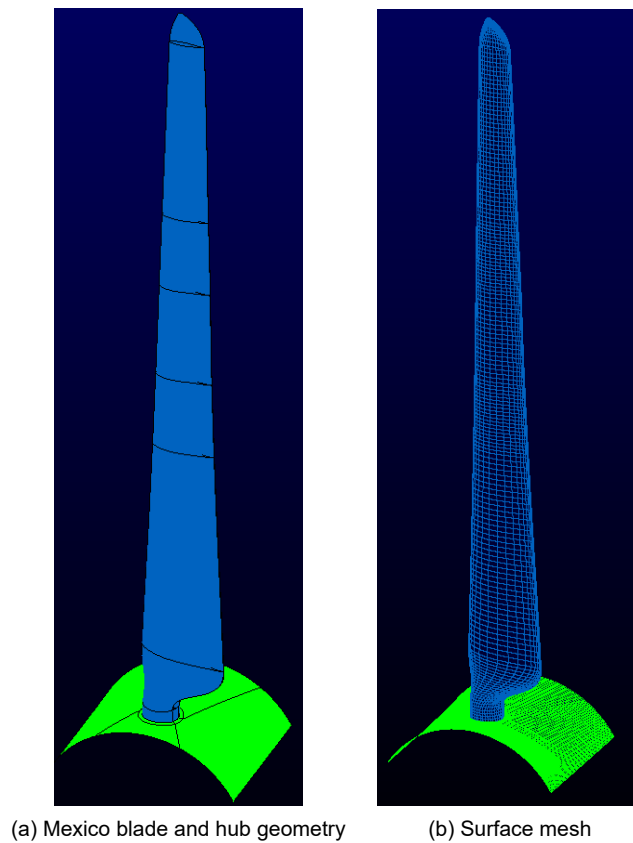
Table 1: Simulated conditions from [2]

Operational state	Wind speed (Uinf) [m/s]	Rotor speed [RPM]	Tip speed ratio [-]	Tinf [°C]	Pinf [Pa]	Density [kg/m^3]
Turbulent wake	10.05	425.1	10.0	20.480	101398	1.197
Design point	15.06	425.1	6.7	21.760	101345	1.191
Separated flow	24.05	425.1	4.2	21.100	101407	1.195

Figure 2: Multi-block grid structure and domain size (R=2.25m)
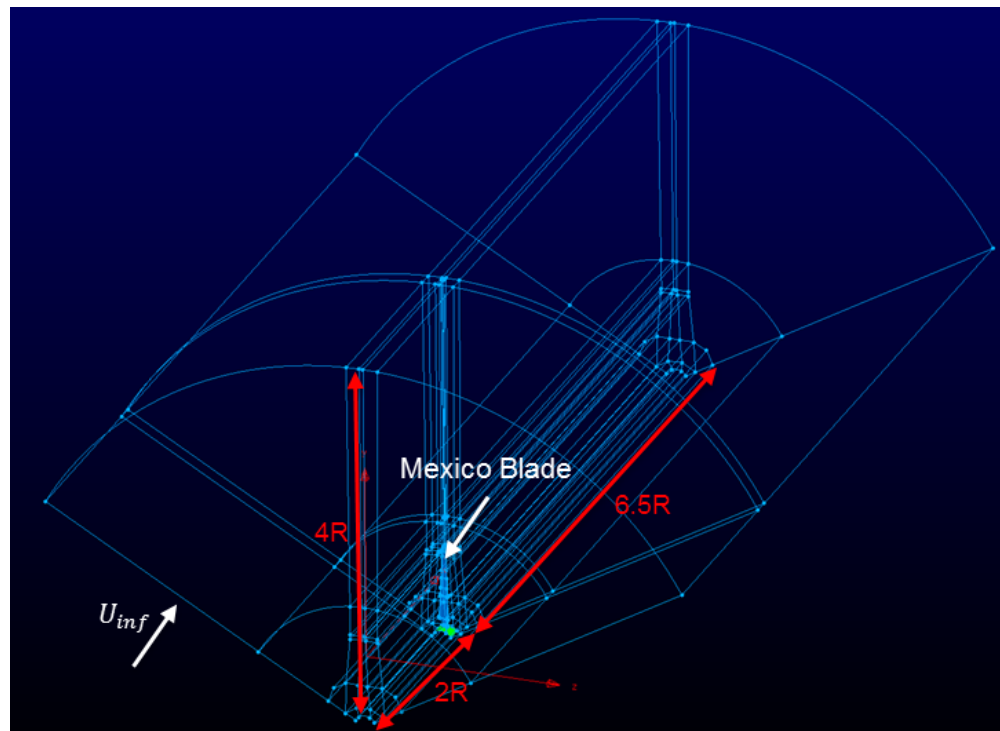
2.1 Computational grid

A constant numerical grid consisting only of hexahedral elements was used with both steady solvers. The simulations modeled the axi-symmetric representation of rotor (single blade) at three different uniform wind speeds. The grid was generated with the Pointwise software, consisting solely of hexahedral elements. The multi-block grid topology and axial grid resolution is shown on Figure 2 and Figure 3a respectively. The grid composed of total 7.1 million hexa elements. An O-H grid topology (Figure 3b) with 47 elements in chord-wise and 191 elements in span-wise direction (Figure 1b) was used with a wall cell height of 1E-6m. The domain extent was considered as 2 and 6.5 times the blade radius (R=2.25m) up and downstream of the rotor plane respectively, while the domain extent was placed at 4R (Figure 2).

Because SU2 was limited to running only on a single node (at the time of writing this report), a coarse grid was selected. In the present context of the study, a mesh or domain extent sensitivity investigations were not performed. It is noted that the considered resolution is a lot coarser than conventional rotor simulation grids (>20million). Additionally it was noted that SU2 was failing to start the simulation for any larger grid using a rotating reference frame.

2.2 Solver

As stated before 2 solvers have been applied: OpenFOAM and SU2.

2.2.1 OpenFOAM - Version: 5.0

In OpenFOAM, the SimpleFoam solver is used. The name comes from the fact that SimpleFoam uses the Semi-Implicit Method for Pressure-Linked Equations (SIMPLE) algorithm of Patankar and Spalding to enforce the pressure/velocity coupling. It is a

Figure 3: Axial and sectional resolution of the grid

| (a) Axial slice | (b) Sectional slice |
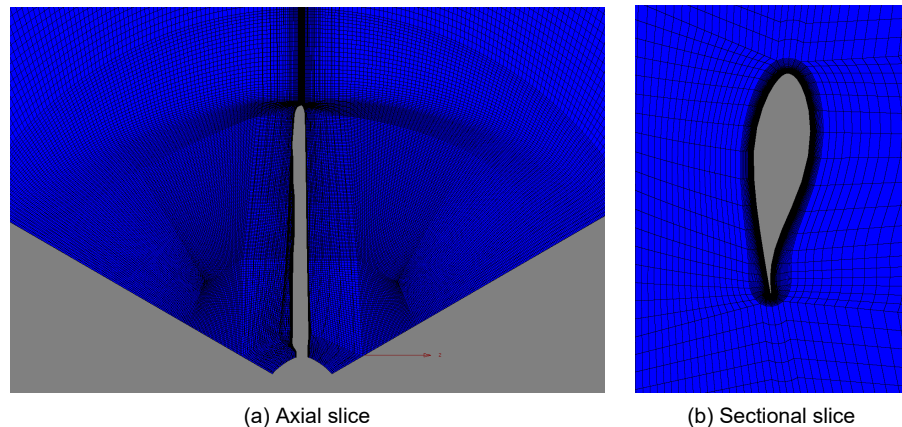
steady-state solver for incompressible turbulent flows. It can be used with a variety of turbulence models which are available in OpenFOAM. For this investigation, and for the sake of comparison with SU2, the RANS kOmegaSST turbulence model is selected. The momentum equations are solved using the 2nd order bounded Gauss linearUpwind scheme. The turbulence closure relations are solved using the bounded Gauss limitedLinear numerical scheme that limits towards 1st order upwind in regions of rapidly changing gradient, while other parts of the domain are resolved using 2nd order linear scheme to achieve greater numerical stability.

OpenFOAM also allows one to choose which specific solver should be used for each of the equations describing the system.

- The momentum, k and omega equations:

  The smoothSolver is used for the momentum equation and for the k and omega equations with a GaussSeidel (Diagonal incomplete-Cholesky) smoother. This particular configuration assured good convergence in the conducted tests.

- The pressure equation:

  For the pressure equation, the GAMG (Geometric-algebraic multi-grid) solver is chosen. GAMG multi-grid solver also requires a smoother for its operation, thus once again GaussSeidel smoother was used with GAMG to ensure a faster convergence. The size of the initial coarse mesh is specified through in the nCellsIn-CoarsestLevel entry, which was specified to be 800 based on 24cpu computations. The agglomeration of cells is performed by the selected FaceAreaPair method.

OpenFOAM can solve both moving reference frames and moving meshs, in the present simulations the rotating reference frame option is used to solve for the Mexico rotor, this also allows a direct comparison with SU2. Convergence criteria is set that the normalized residual is reduced by five orders of magnitude from the initial value. For high wind speeds it was not always possible to reduce five order of magnitude (Figure 4), and in this case the results are averaged over a sustained period of iterations, typically 500 iterations.

Each OpenFoam iteration typically computes in 15 seconds on 24cpu nodes and convergence is achieved within 20k iterations, which result in a reasonable computational time within a week.

Figure 4: OpenFOAM RMS residuals plots

(a) Wind speed = 10m/s   (b) Wind speed = 24m/s
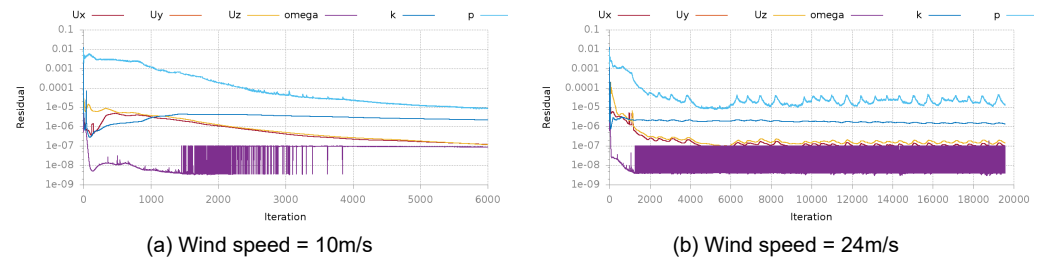
2.2.2   *SU2 - Release 6.0.0 "Falcon"*

In SU2, the compressible RANS solver is used. It is a steady-state solver for compressible turbulent flows. Its solves the steady compressible NS equations, with ideal gas law to model the thermodynamic state of STANDARD_AIR (Specific gas constant: 287.058 N.m/kg.K.). The Menter's SST turbulence model is used for all SU2 simulations.

The Jameson-Schmidt-Turkel (JST) 2nd order numerical scheme was used to solve the convective fluxes, while a first order SCALAR_UPWIND method was employed to solve the turbulence closure equations. Both the convective and turbulence models were computed with the VENKATAKRISHNAN slope limiter using EULER_IMPLICIT time discretisation. Spatial gradients were computed using the GREEN_GAUSS numerical method with the CFL(Courant–Friedrichs–Lewy) number of 5.

In the present simulations the rotating reference frame option within SU2 is used to solve for the Mexico rotor. Convergence criteria is set similar to OpenFOAM were the normalized residual is reduced by five orders of magnitude from the initial value. Based on this criteria SU2 converges in around 200k number of iterations (Figure 5), which is one order of magnitude higher number of iterations than with OpenFOAM. In all case the results are averaged over a sustained period of iterations, typically 500 iterations.

Each SU2 iteration computes in 16 seconds using 24cpus, which results in a very long 37days computational time. At the OpenFOAM equivalent of 20k iterations, SU2 simulations achieved a reduction of RMS residuals of only two order of magnitude (Figure 5).

Figure 5: SU2 RMS residuals plots

(a) Wind speed = 10m/s   (b) Wind speed = 24m/s
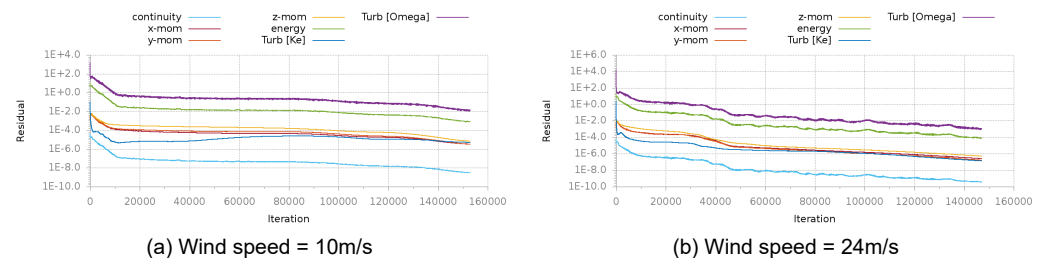
2.3   Boundary conditions

Major differences between the two codes concerning the boundary condition specification are related to the usage of wall functions. OpenFOAM offers variety of wall functions to model the flow close to the wall, while SU2 resolves the boundary layer (BL) based on the grid elements. The kqRWallFunction and omegaWallFunction are

Table 2: Simulated boundary conditions

Boundary patch	OpenFOAM	SU2
Inlet	Freestream Velocity	Freestream Velocity
Outlet	Freestream Pressure	Freestream Velocity
Top	Free slip	Freestream Velocity
Sides	Periodic	Periodic
Blade	No Slip (with wall functions)	No Slip (grid resolved BL)
Hub	No Slip (with wall functions)	No Slip (grid resolved BL)

used to model the non slip wall boundaries(blade and hub patches) within the presented OpenFOAM simulations.

OpenFOAM also offers a stable outlet boundary condition that actively switches to prevent back flow while maintaining a prescribed outlet pressure. SU2 on the other hand offers a pressure boundary that allows back flow, severely delaying the convergence time, thus velocity boundary conditions were applied for the SU2 outlet boundary. The boundary conditions set for both codes are as detailed in Table 2.

3   Results and Discussion

Comparison of the CFD computed thrust and power coefficient against the measured values are shown in Table 3, while the detailed blade pressure and flow field velocity values are compared in Appendix A-D. Another CFD results from DTU[3] using their ElipSys3D solver was also added for comparison. In some plots an average of all 'CFD' data from the Mexnext project is also incorporated for assessing the initial results to date. Its is once again noted that, the simulations were crudely setup to establish an initial numerical result with stability and one should take drawing conclusions from the following discussion.

Assessment of the detailed results, such the blade pressure distribution (Appendix A) shows that a better agreement is established between the SU2 results and the measurements, which is also in correspondence with the DTU results. By rare coincidence the OpenFOAM results at 60% blade span agrees better with the measurements than the SU2 or DTU results. However it was indicated in the final report of Mexnext phase 3 [3], that there are some open questions at this radius, as all CFD data from the Mexnext campaign consistently over predicted suction pressure from the measurements.

Comparing the integrated blade surface loads (Table 3), shows that the OpenFOAM thrust values agree well with the measurements (<2%), while SU2 results show differences up to 14% at the 10m/s wind speed. In view of the disagreement in local loads as described above this is unexpected and can be explained by compensating errors. Both solvers over predict the power production of the turbine, except Open-FOAM at the separated flow regime (24m/s). Additional Cdax and Cp values were also computed using only the pressure distribution from five radial location: 25, 35, 60, 82 and 92% blade radius. This comparison is shown in Figure 6 and 7, which again suggests that the integrated blade thrust and torque values are unexpectedly captured better with OpenFOAM than SU2. This clearly suggests that the quality of CFD results should not be assessed only using the integrated values, as it is seen for this case where OpenFOAM's over and under predicted local pressure values are easily disregarded within the integrated values.

The axial traverse data comparison (Appendix B), clearly shows the effect of the very small domain extent, as the prescribed boundary values are established at x=-4m (1m downstream of the inlet boundary). With larger domain extent, one can better resolve the induction from the rotor and achieve the realistic flow field as measured. It is also clear that the SU2 results agree better with the DTU results and the measurements, while a larger discrepancy is seen with the OpenFOAM results, especially in the rotor wake region.

The effect of the poor domain extent is also visible in the radial traverse flow velocities, specifically the u component is constantly over predicted by both solver. However, the non zero w component before the rotor plane (x=-0.3m) is more cause for concern as it indicates a spurious swirl component being introduced before the flow actually reaches the rotor plane (Figure 63-64).

Table 3: Mexico rotor thrust (Cdax) and power (Cp) coefficient

Wind Speed	Cdax			Cp		
[m/s]	OpenFOAM	SU2	Exp	OpenFOAM	SU2	Exp
10	1.027	1.160	1.016	0.337	0.365	0.316
15	0.802	0.853	0.775	0.447	0.464	0.438
24	0.387	0.433	0.395	0.205	0.238	0.240

Figure 6: Comparison of thrust values computed from pressure distribution
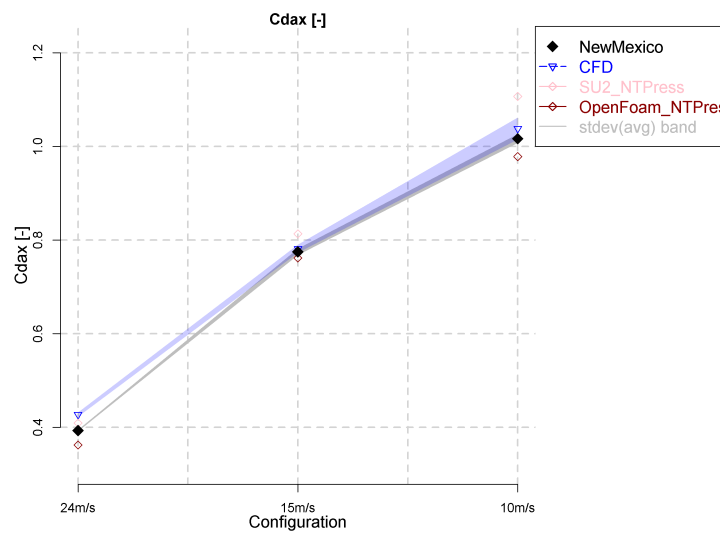
Figure 7: Comparison of power coefficients computed from pressure distribution
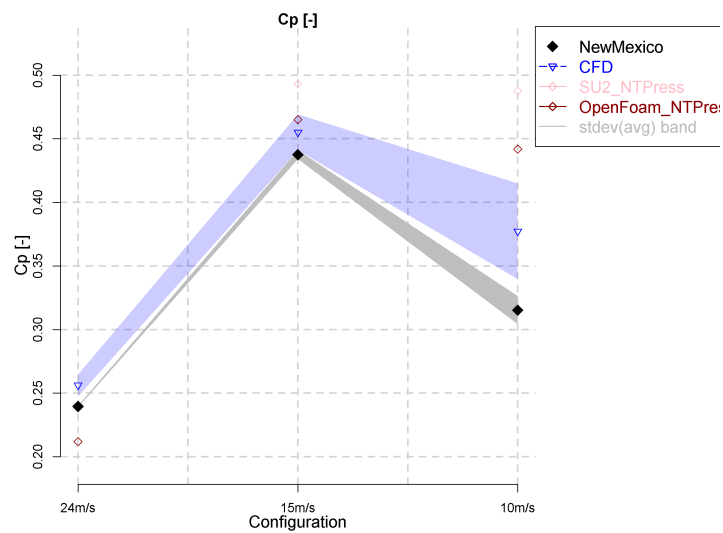
4   Conclusion

OpenFoam and SU2 have successfully been applied to reproduce the New Mexico wind tunnel experiment at various operational conditions using a relatively crude mesh. Based on this initial investigation, it was clear that OpenFOAM is able to compute the flow field at much faster rate than SU2's version to date as the current SU2 implementation could not be parallelised efficiently. However, the flow field and the blade pressure values are relatively better resolved with SU2.

It is important to note that one should not draw any final conclusions based on these results - as improving the grid and domain extent alone will result in different performances from these two solvers. A grid independent solution from both solvers is required to establish a tangible conclusion on the solvers. Nevertheless based on this initial results to date, SU2's compressible solver appears to be a versatile tool for wind energy applications.

A   Comparison plots: Chordwise pressure distribution

Figure 8: Chordwise pressure distribution at 25% of the blade for the freestream velocity of 10m/s
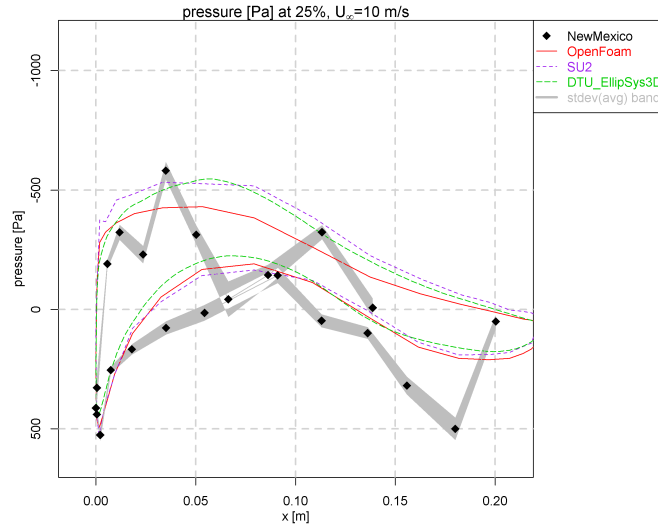
Figure 9: Chordwise pressure distribution at 25% of the blade for the freestream velocity of 15m/s
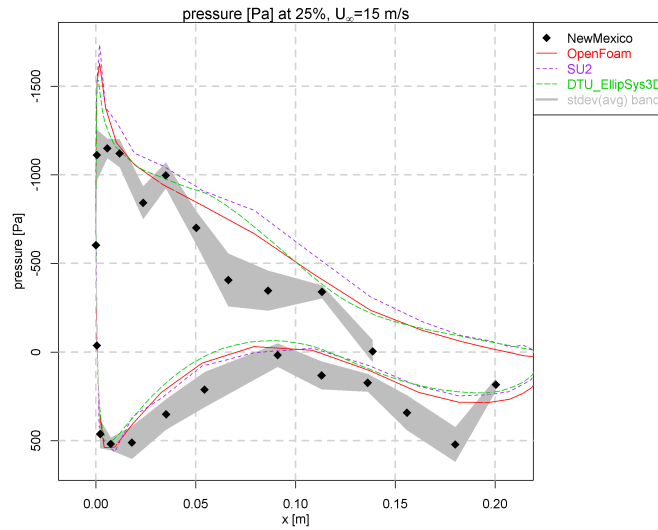
Figure 10: Chordwise pressure distribution at 25% of the blade for the freestream velocity of 24m/s
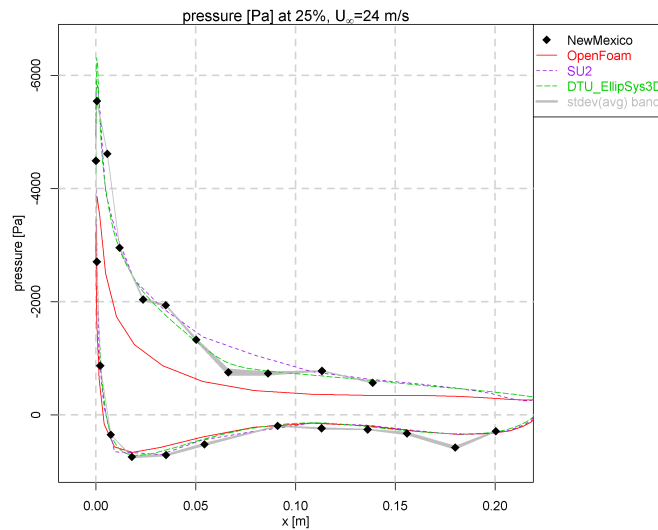
Figure 11: Chordwise pressure distribution at 35% of the blade for the freestream velocity of 10m/s
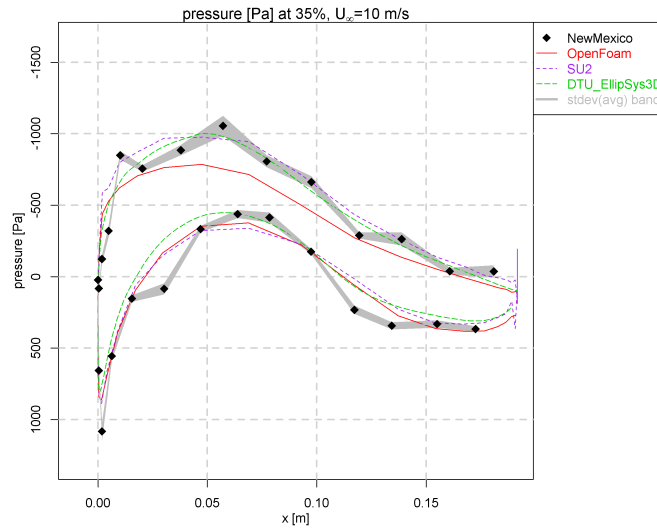
Figure 12: Chordwise pressure distribution at 35% of the blade for the freestream velocity of 15m/s
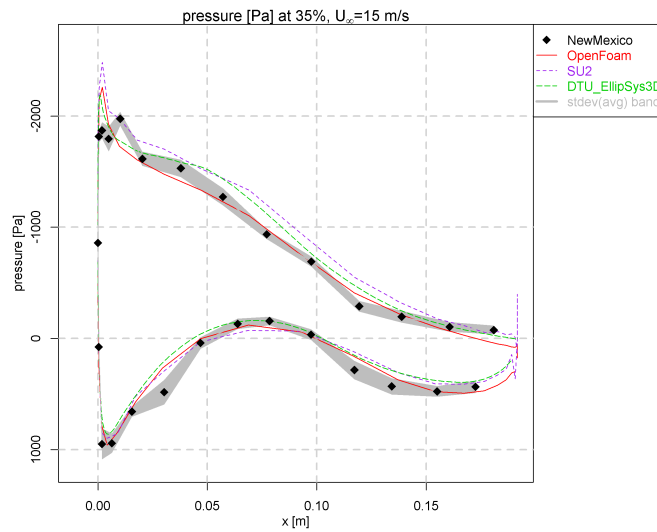
Figure 13: Chordwise pressure distribution at 35% of the blade for the freestream velocity of 24m/s
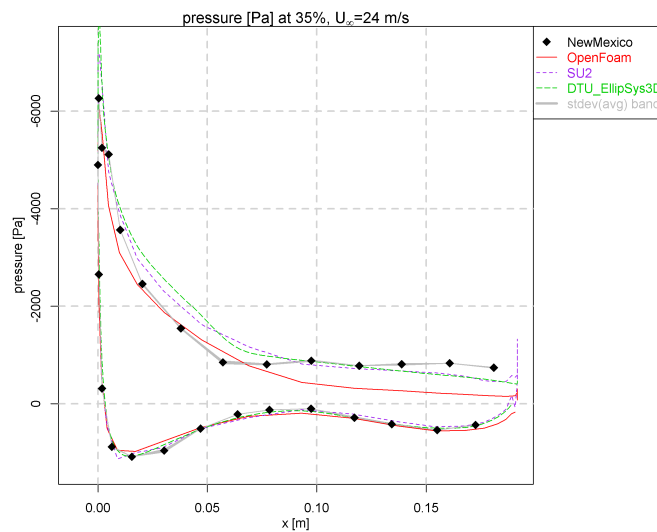
Figure 14: Chordwise pressure distribution at 60% of the blade for the freestream velocity of 10m/s
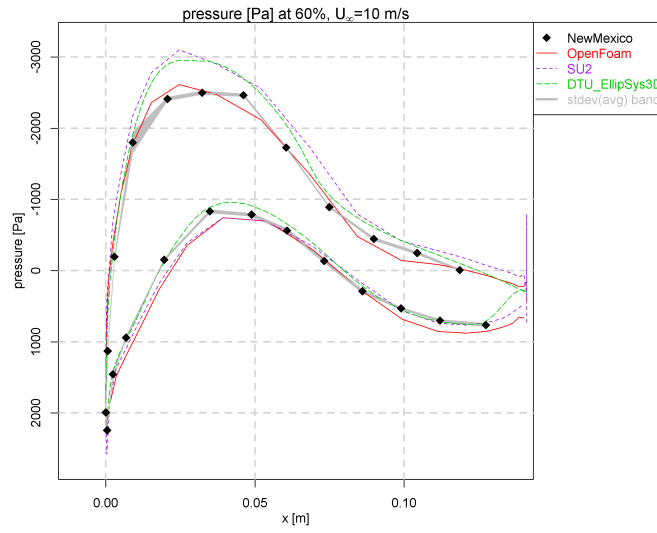
Figure 15: Chordwise pressure distribution at 60% of the blade for the freestream velocity of 15m/s
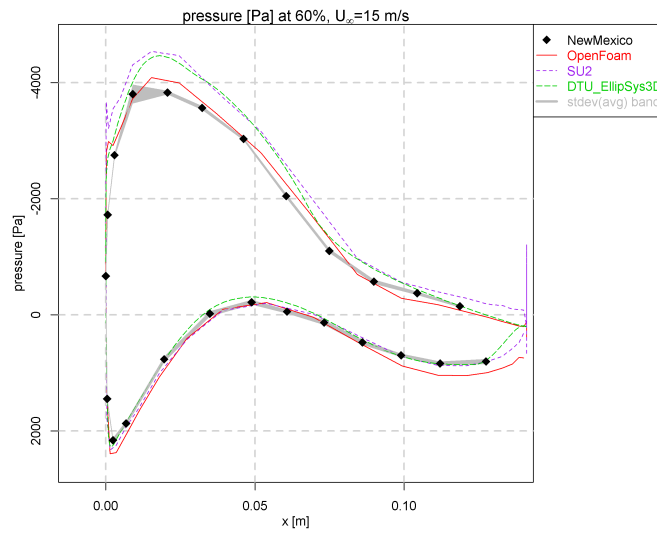
Figure 16: Chordwise pressure distribution at 60% of the blade for the freestream velocity of 24m/s
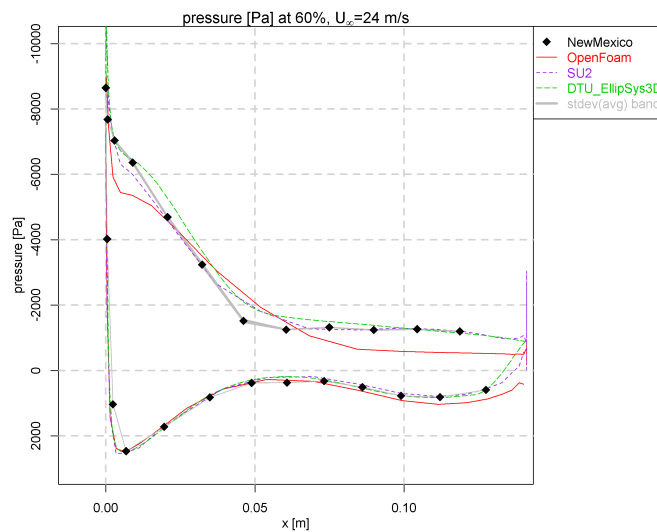
Figure 17: Chordwise pressure distribution at 82% of the blade for the freestream velocity of 10m/s
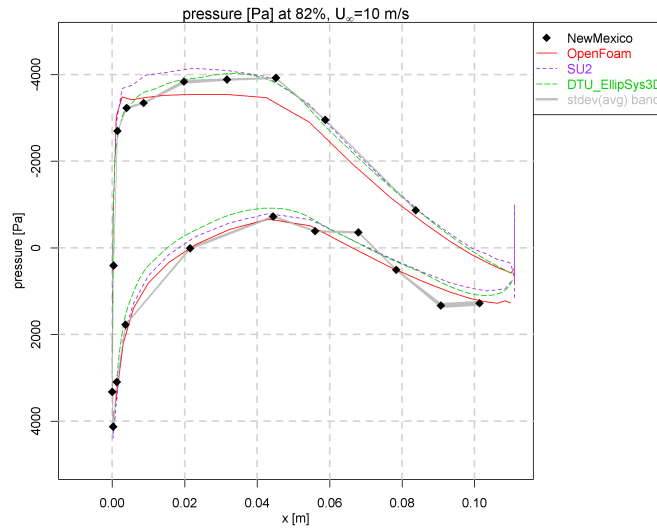
Figure 18: Chordwise pressure distribution at 82% of the blade for the freestream velocity of 15m/s
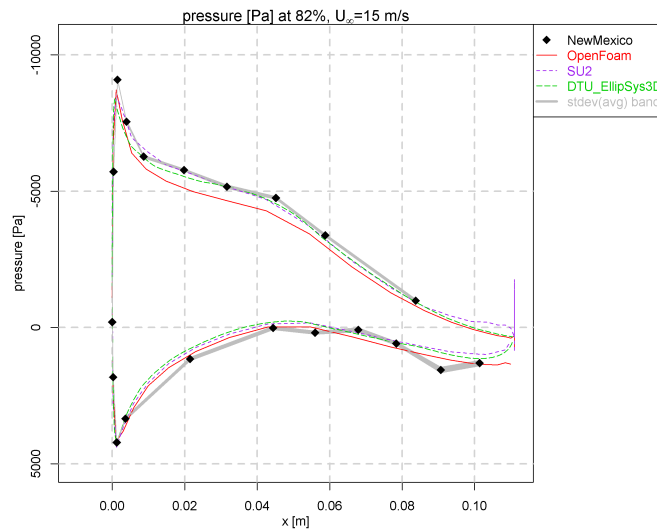
Figure 19: Chordwise pressure distribution at 82% of the blade for the freestream velocity of 24m/s
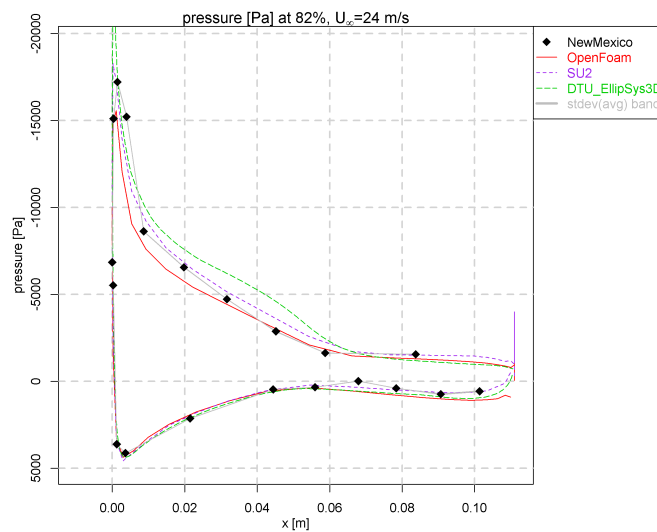
Figure 20: Chordwise pressure distribution at 92% of the blade for the freestream velocity of 10m/s
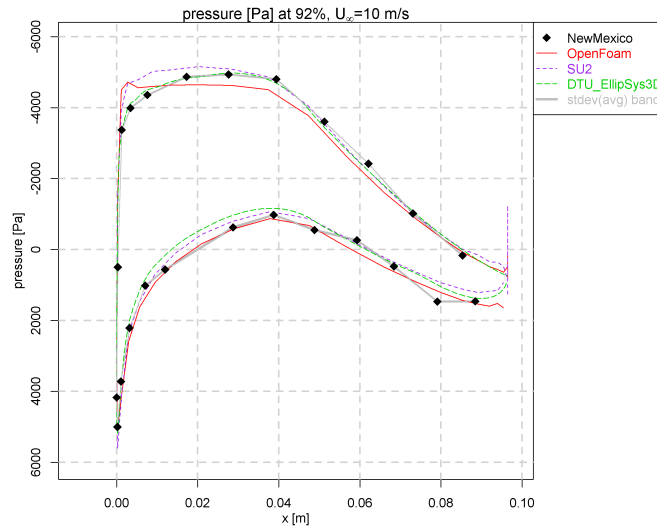
Figure 21: Chordwise pressure distribution at 92% of the blade for the freestream velocity of 15m/s
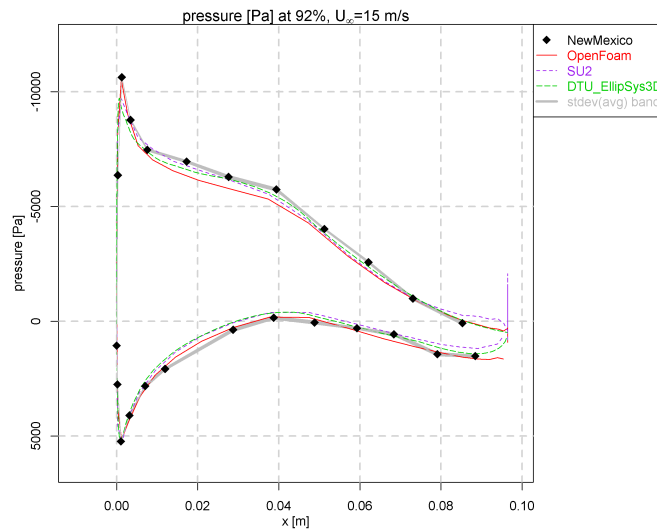
Figure 22: Chordwise pressure distribution at 92% of the blade for the freestream velocity of 24m/s
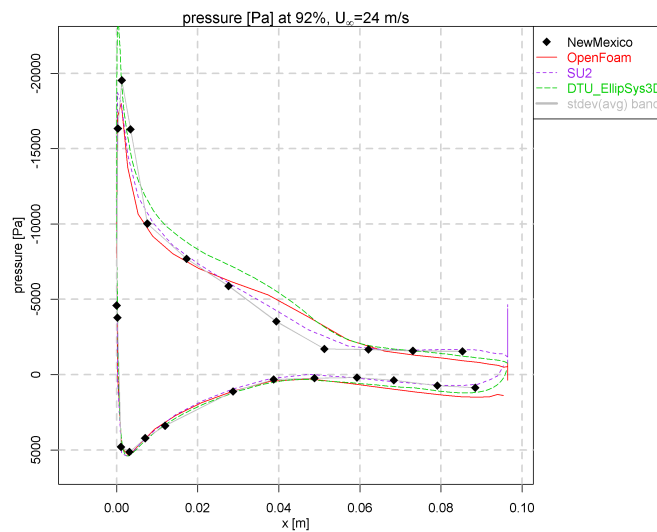
B   Comparison plots: Blade normal and tangential load distribution computed from pressure distribution

Figure 23: Blade normal force distribution for the freestream velocity of 10m/s
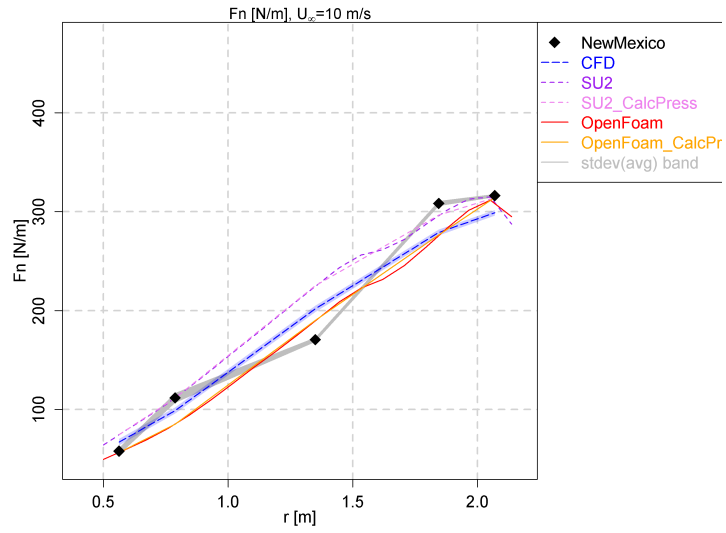
Figure 24: Blade normal force distribution for the freestream velocity of 15m/s
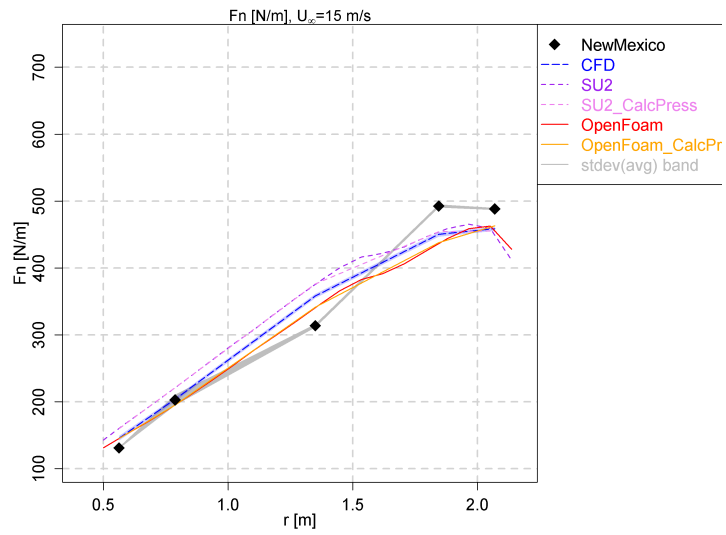
Figure 25: Blade normal force distribution for the freestream velocity of 24m/s
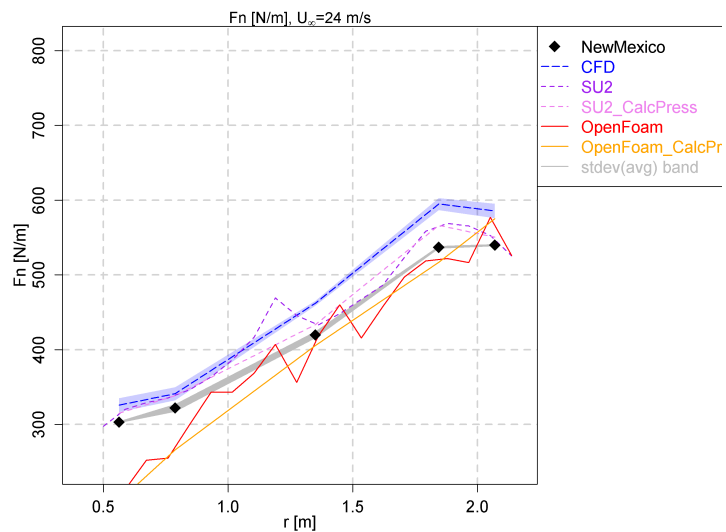
Figure 26: Blade tangential force distribution for the freestream velocity of 10m/s
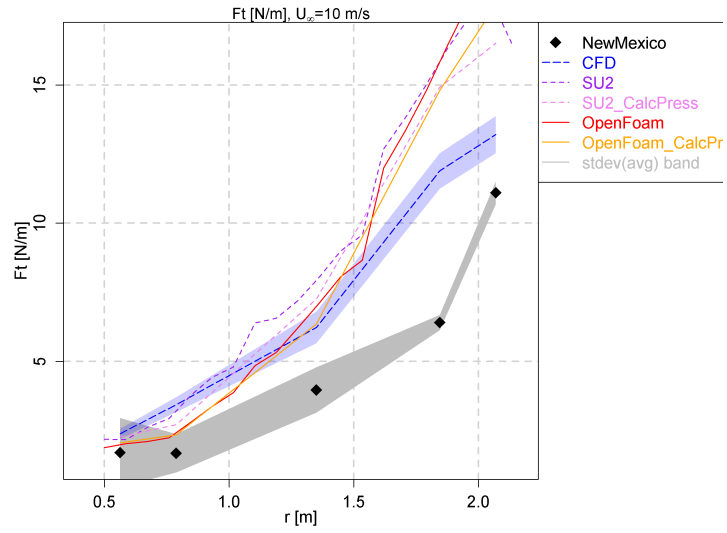
Figure 27: Blade tangential force distribution for the freestream velocity of 15m/s
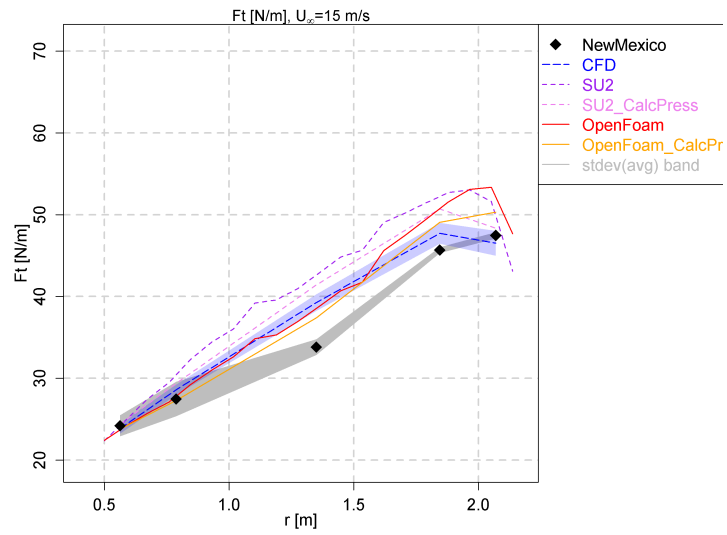
Figure 28: Blade tangential force distribution for the freestream velocity of 24m/s
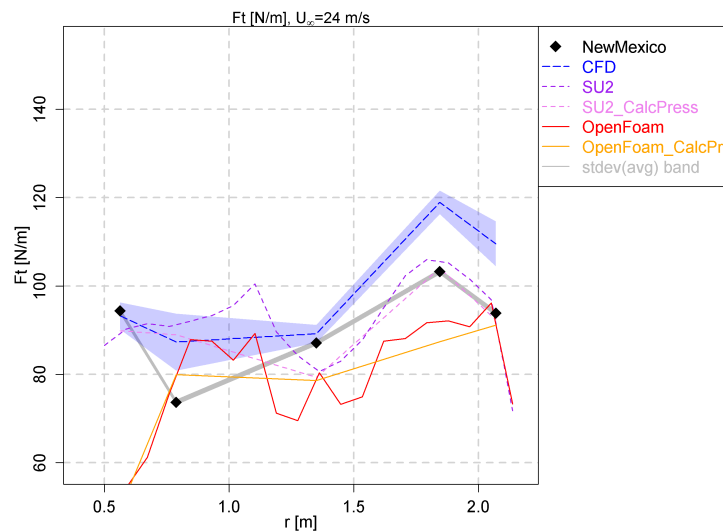
C   Comparison plots: Axial Traverse Velocity

Figure 29: Axial traverse velocity u at blade radius 0.5m for the freestream velocity of 10m/s
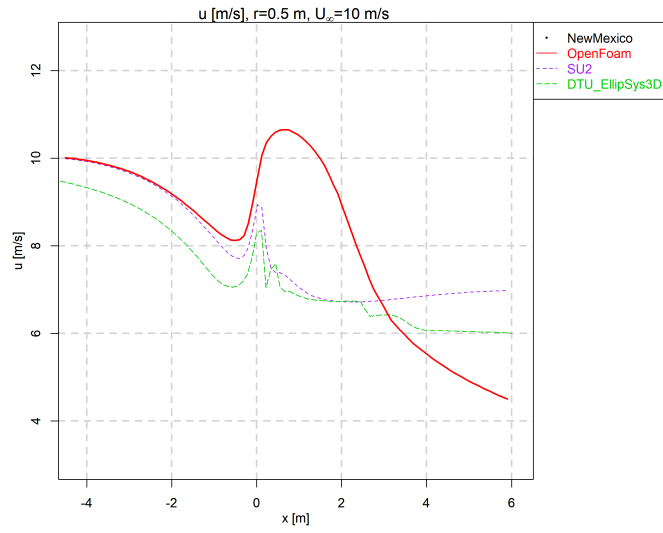
Figure 30: Axial traverse velocity u at blade radius 0.5m for freestream velocity of 15m/s
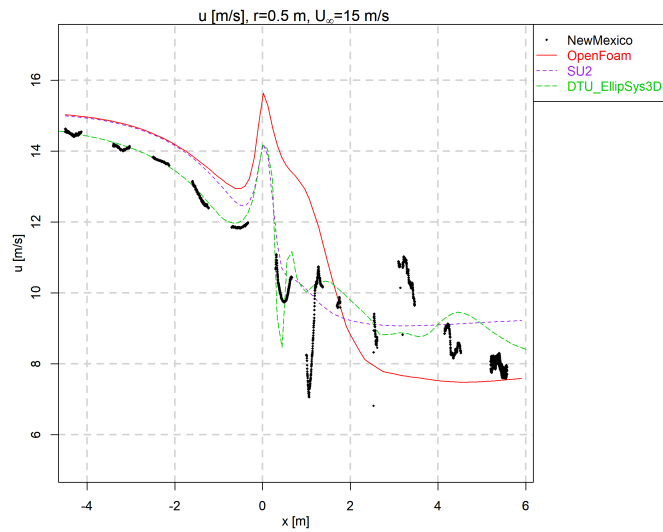
Figure 31: Axial traverse velocity u at blade radius 0.5m for the freestream velocity of 24m/s
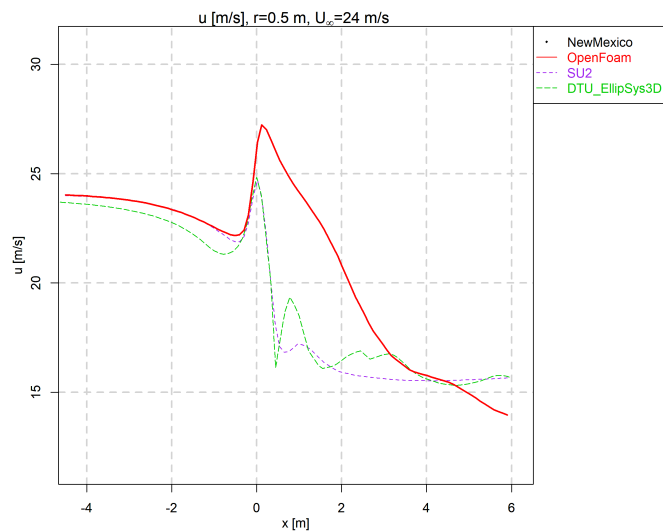
Figure 32: Axial traverse velocity u at blade radius 1.5m for the freestream velocity of 10m/s
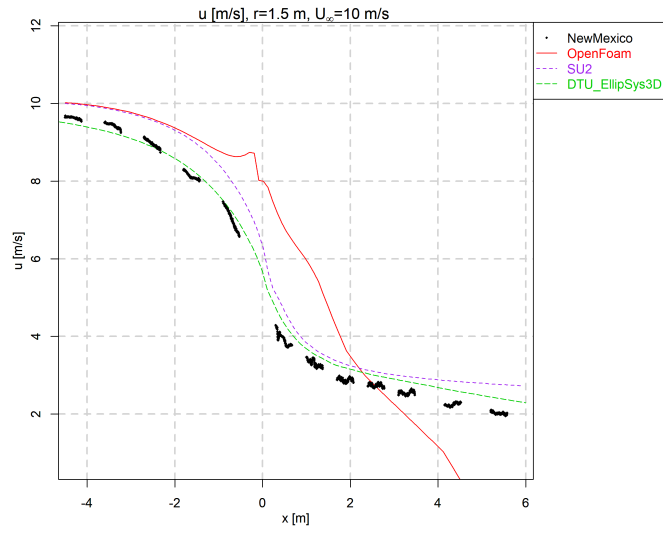
Figure 33: Axial traverse velocity u at blade radius 1.5m for the freestream velocity of 15m/s
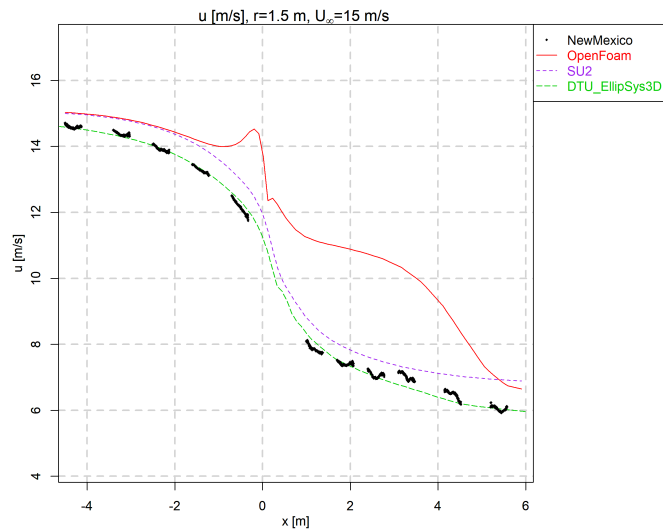
Figure 34: Axial traverse velocity u at blade radius 1.5m for the freestream velocity of 24m/s
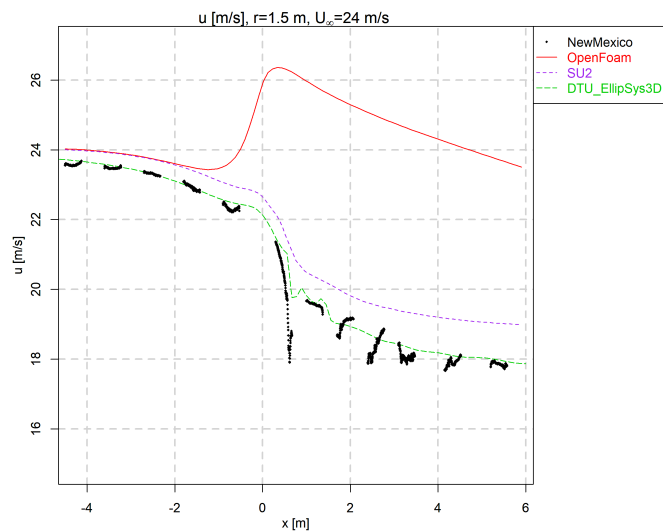
Figure 35: Axial traverse velocity v at blade radius 0.5m for the freestream velocity of 10m/s
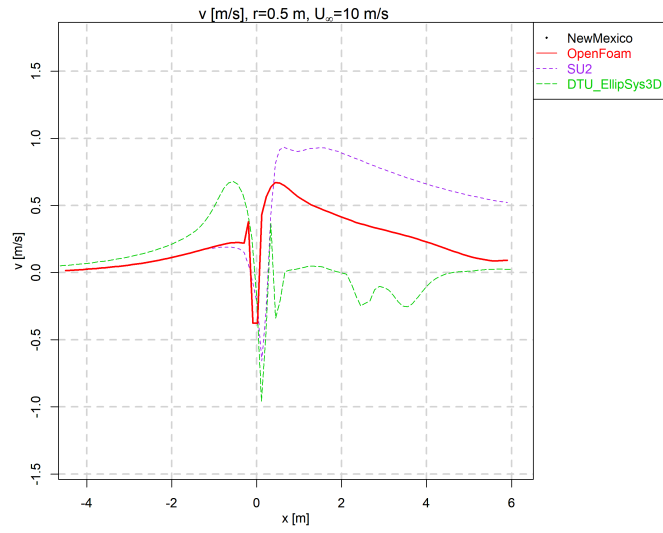
Figure 36: Axial traverse velocity v at blade radius 0.5m for the freestream velocity of 15m/s
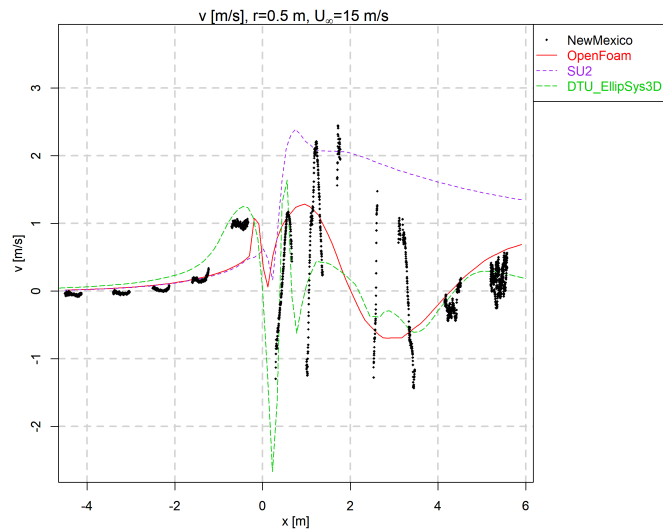
Figure 37: Axial traverse velocity v at blade radius 0.5m for the freestream velocity of 24m/s
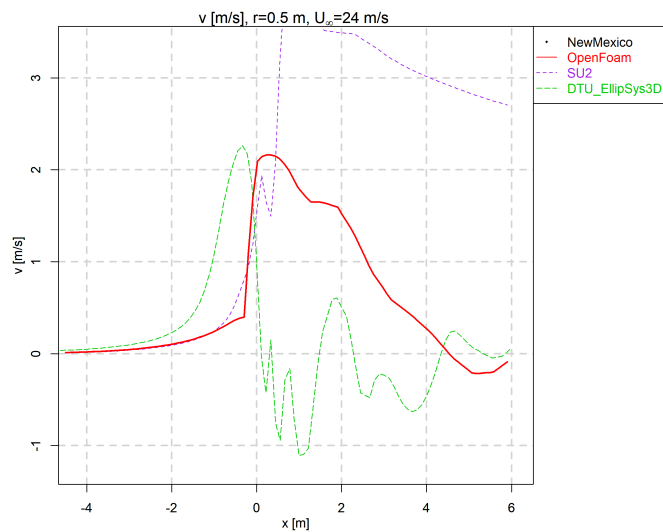
Figure 38: Axial traverse velocity v at blade radius 1.5m for the freestream velocity of 10m/s
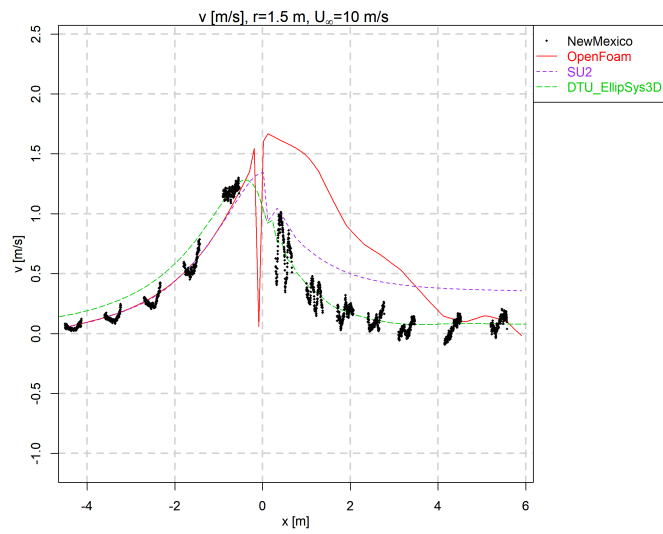
Figure 39: Axial traverse velocity v at blade radius 1.5m for the freestream velocity of 15m/s
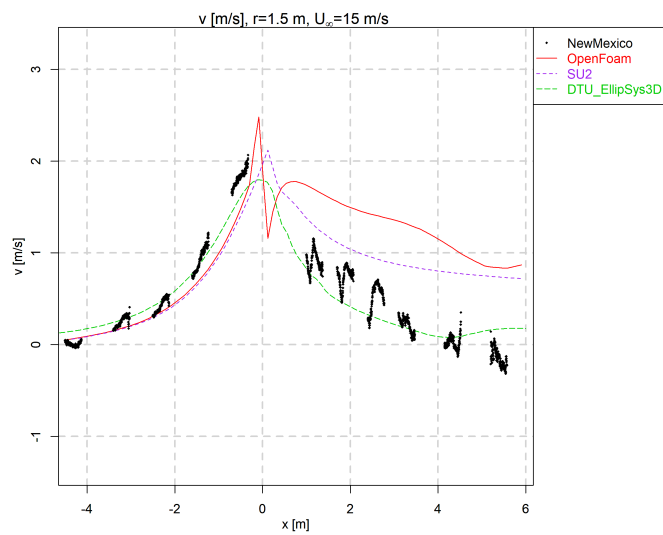
Figure 40: Axial traverse velocity v at blade radius 1.5m for the freestream velocity of 24m/s
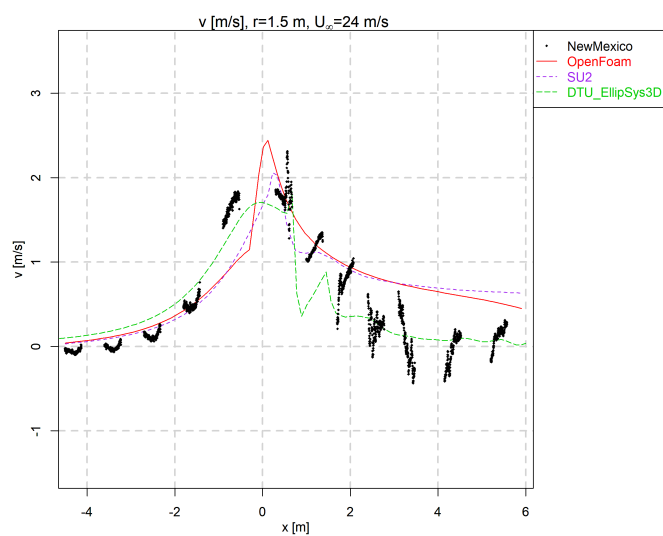
Figure 41: Axial traverse velocity w at blade radius 0.5m for the freestream velocity of 10m/s
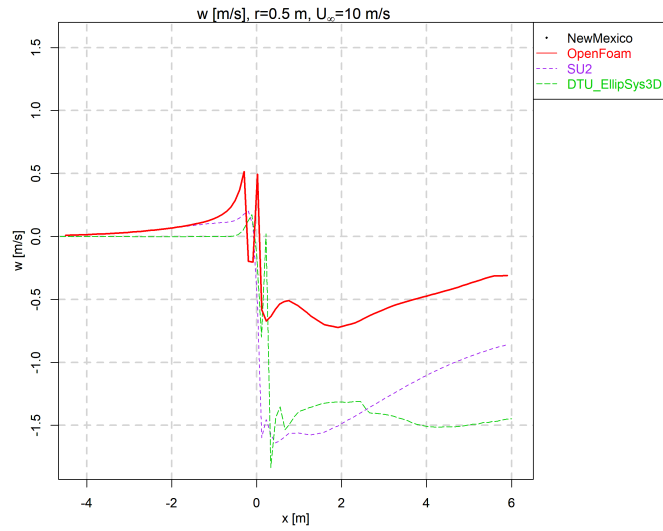
Figure 42: Axial traverse velocity w at blade radius 0.5m for the freestream velocity of 15m/s
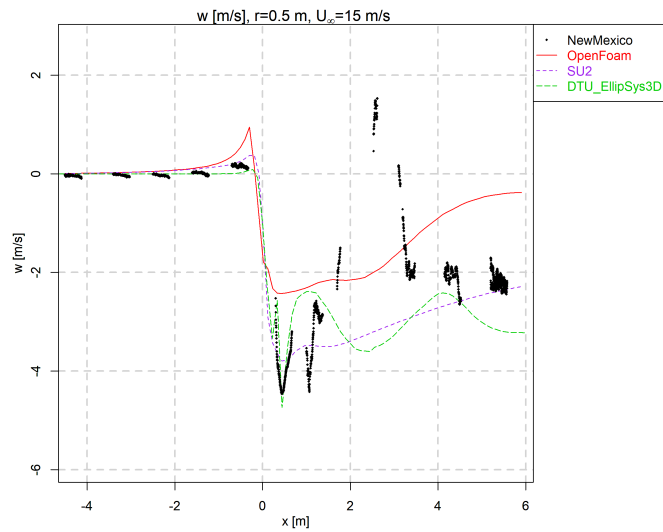
Figure 43: Axial traverse velocity w at blade radius 0.5m for the freestream velocity of 24m/s
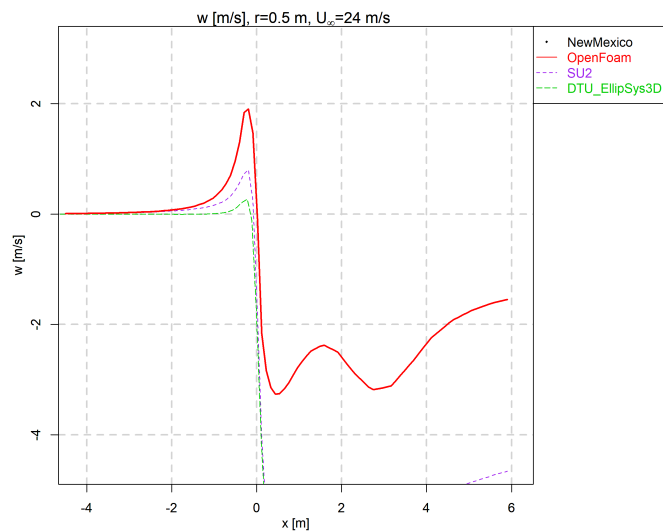
Figure 44: Axial traverse velocity w at blade radius 1.5m for the freestream velocity of 10m/s
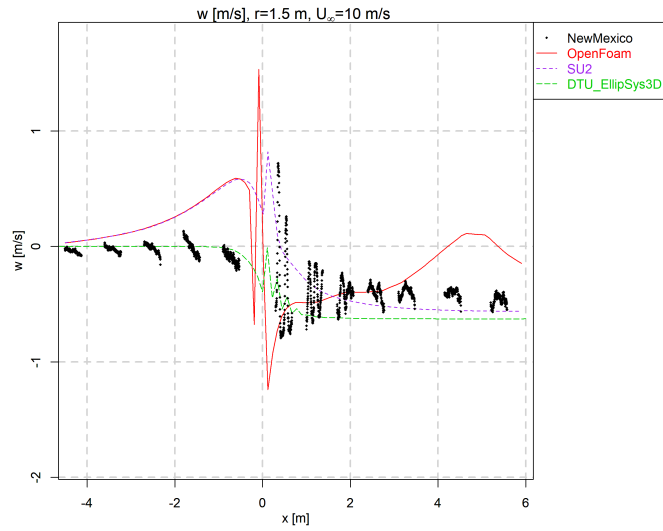
Figure 45: Axial traverse velocity w at blade radius 1.5m for the freestream velocity of 15m/s
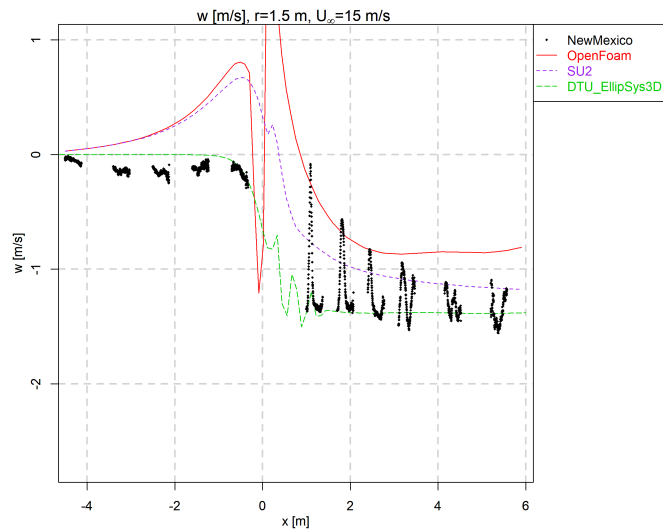
Figure 46: Axial traverse velocity w at blade radius 1.5m for the freestream velocity of 24m/s
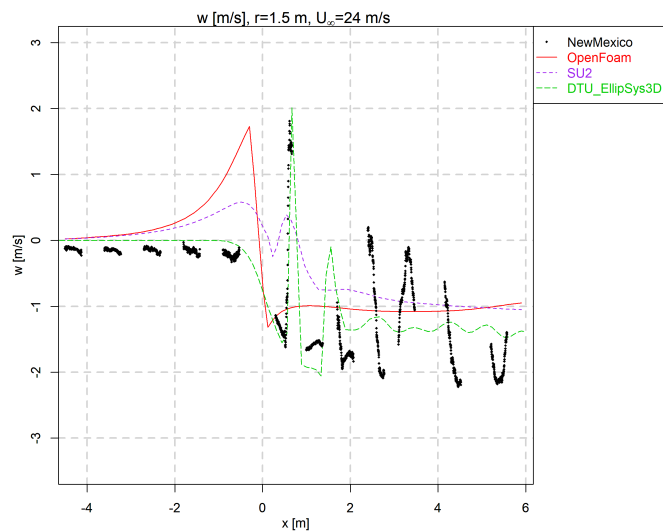
D Comparison plots: Radial Traverse Velocity

Figure 47: Radial traverse velocity u at axial location x=+0.3m for the freestream velocity of 10m/s
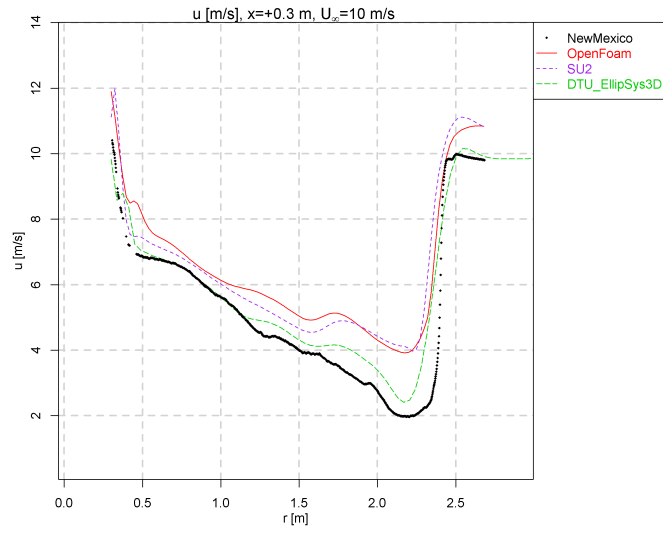
Figure 48: Radial traverse velocity u at axial location x=+0.3m for the freestream velocity of 15m/s
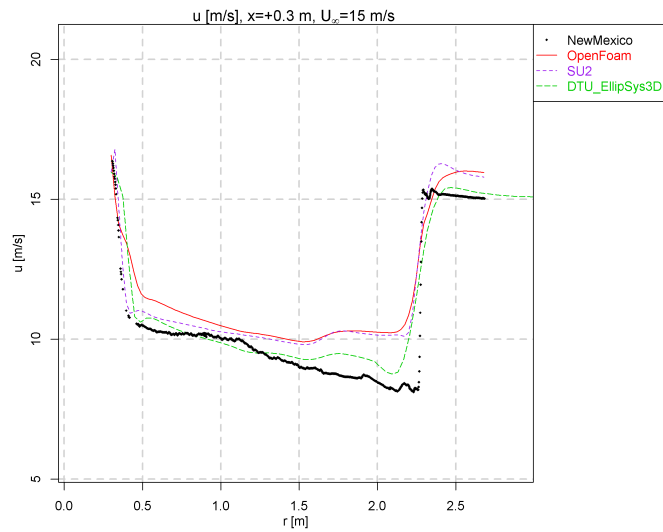
Figure 49: Radial traverse velocity u at axial location x=+0.3m for the freestream velocity of 24m/s
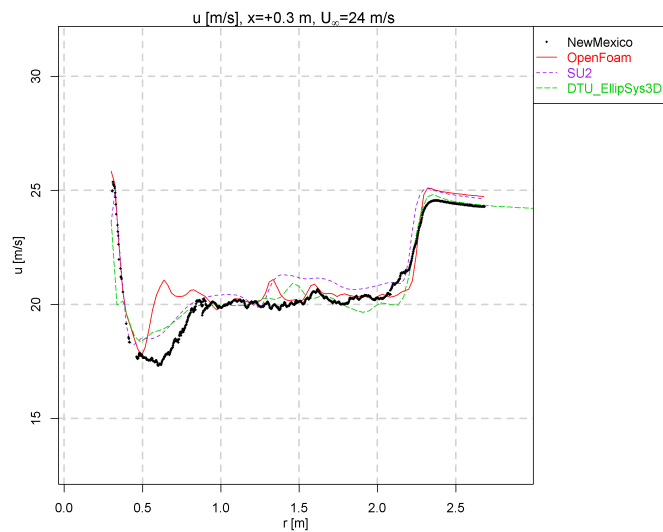
Figure 50: Radial traverse velocity u at axial location x=-0.3m for the freestream velocity of 10m/s
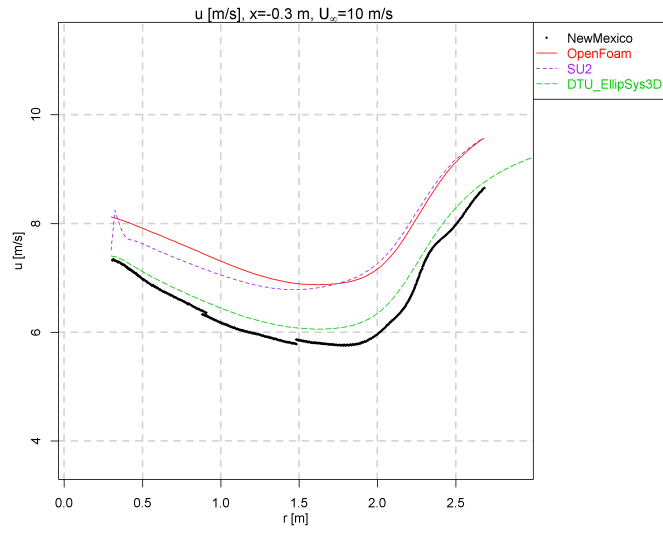
Figure 51: Radial traverse velocity u at axial location x=-0.3m for the freestream velocity of 15m/s
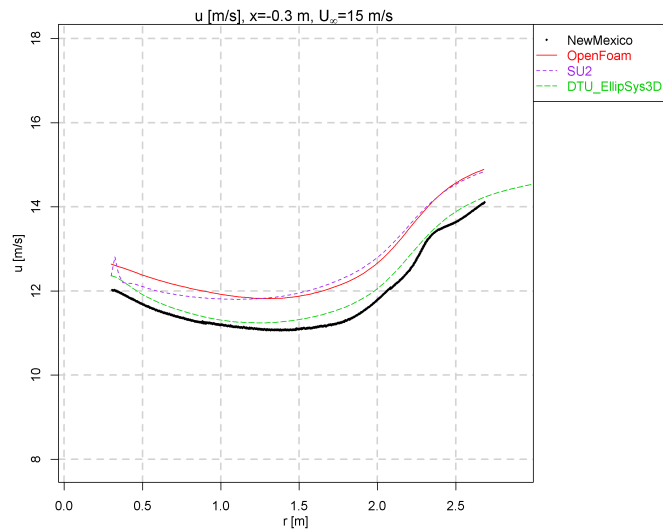
Figure 52: Radial traverse velocity u at axial location x=-0.3m for the freestream velocity of 24m/s
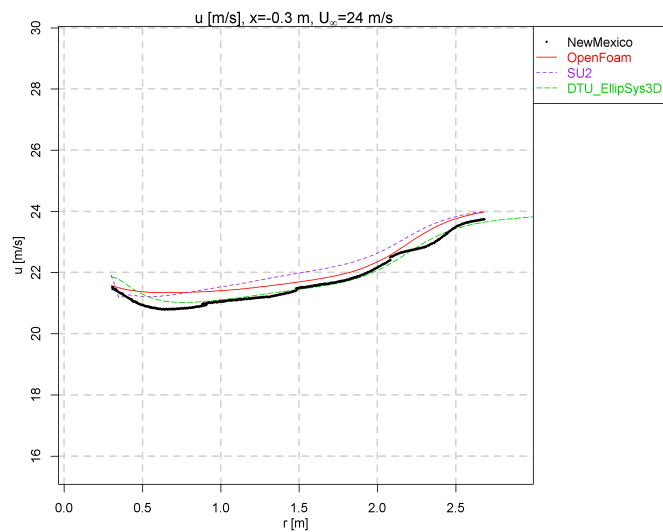
Figure 53: Radial traverse velocity v at axial location x=+0.3m for the freestream velocity of 10m/s
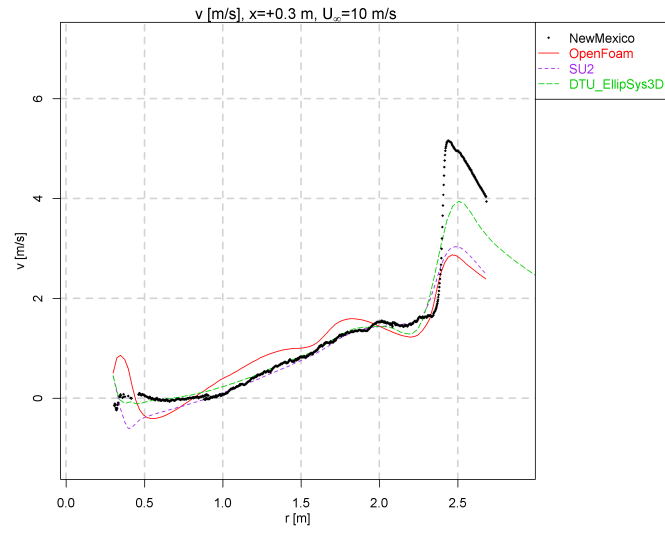
Figure 54: Radial traverse velocity v at axial location x=+0.3m for the freestream velocity of 15m/s
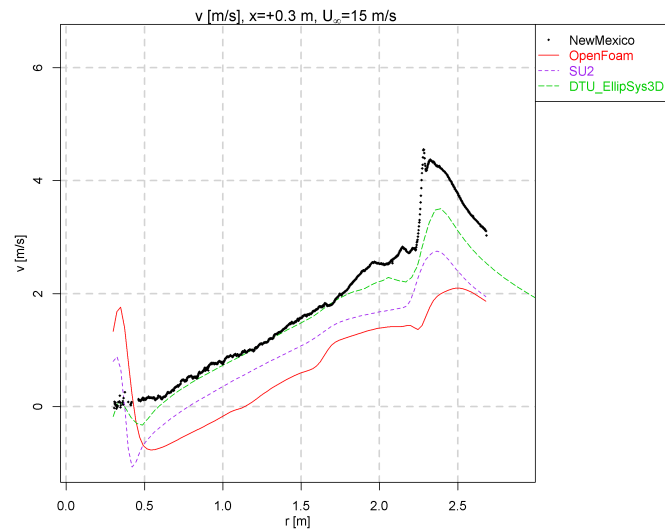
Figure 55: Radial traverse velocity v at axial location x=+0.3m for the freestream velocity of 24m/s
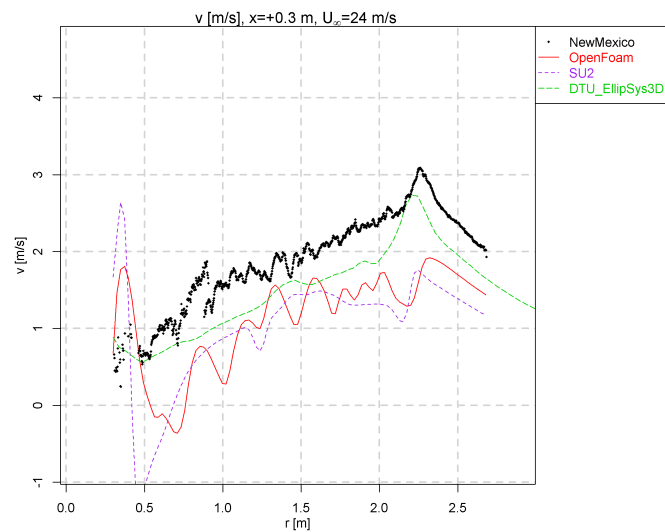
Figure 56: Radial traverse velocity v at axial location x=-0.3m for the freestream velocity of 10m/s
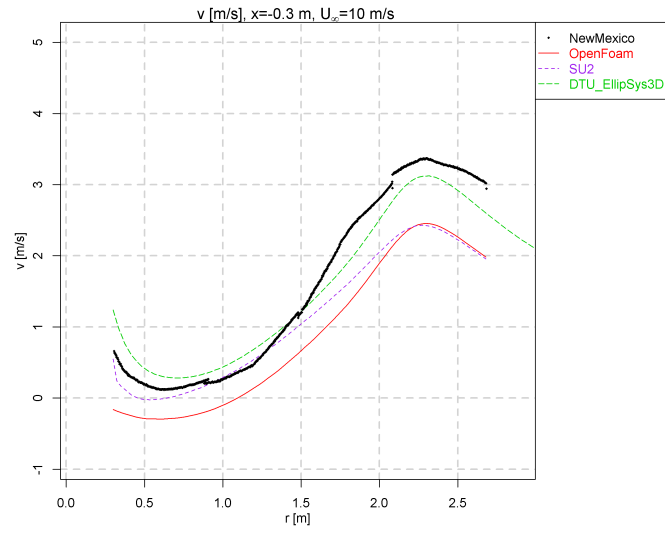
Figure 57: Radial traverse velocity v at axial location x=-0.3m for the freestream velocity of 15m/s
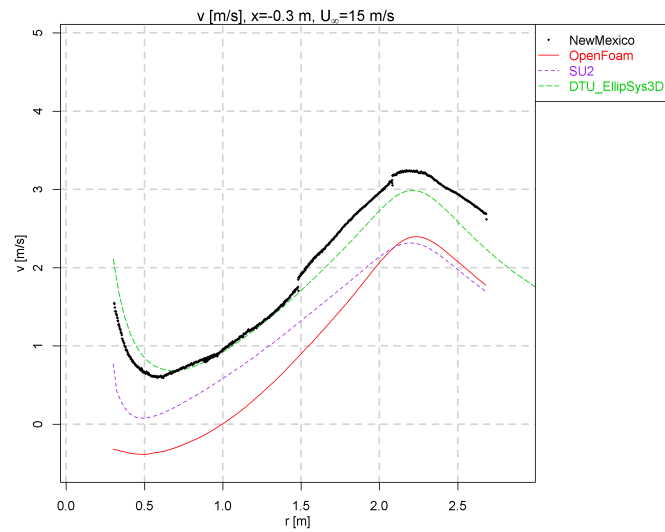
Figure 58: Radial traverse velocity v at axial location x=-0.3m for the freestream velocity of 24m/s
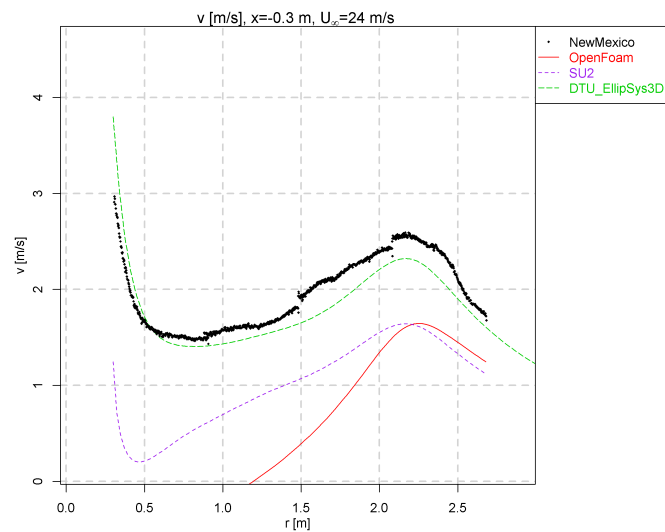
Figure 59: Radial traverse velocity w at axial location x=+0.3m for the freestream velocity of 10m/s
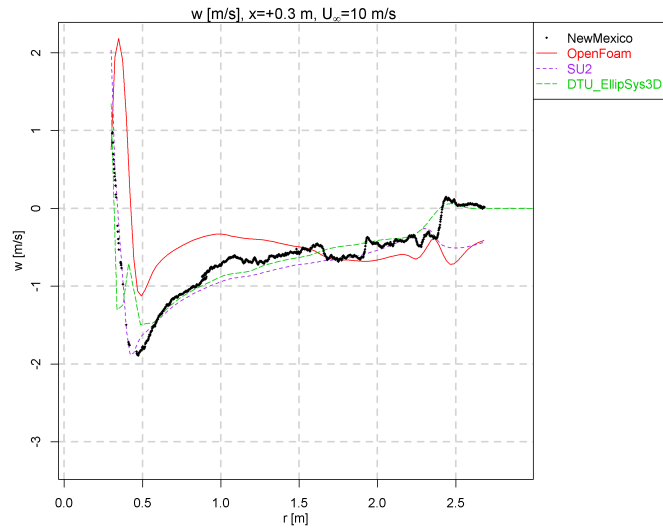
Figure 60: Radial traverse velocity w at axial location x=+0.3m for the freestream velocity of 15m/s
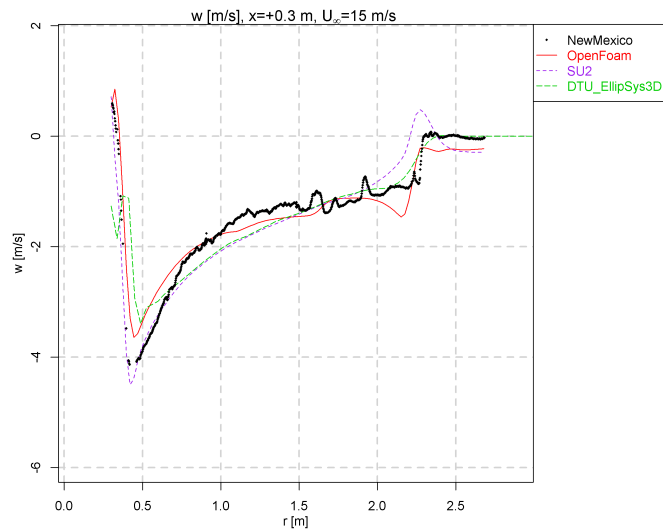
Figure 61: Radial traverse velocity w at axial location x=+0.3m for the freestream velocity of 24m/s
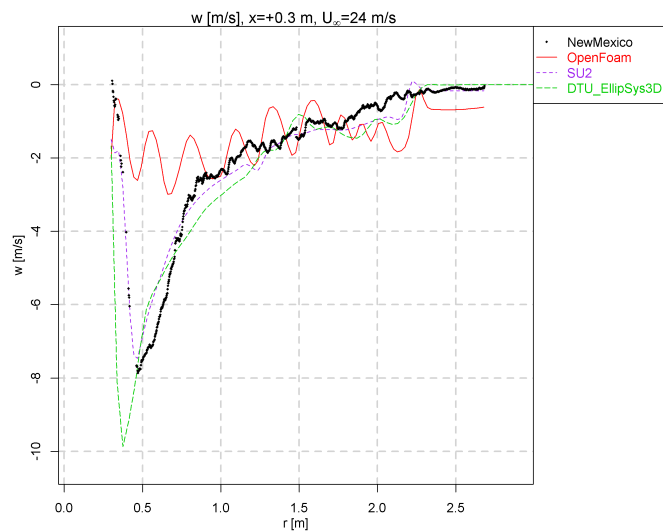
Figure 62: Radial traverse velocity w at axial location x=-0.3m for the freestream velocity of 10m/s
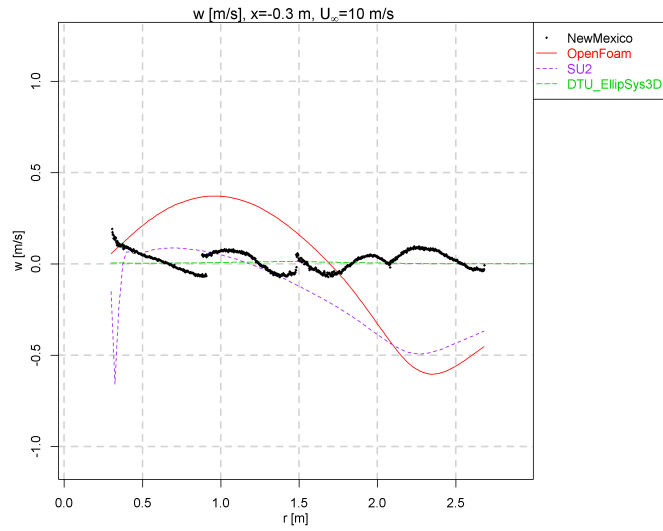
Figure 63: Radial traverse velocity w at axial location x=-0.3m for the freestream velocity of 15m/s
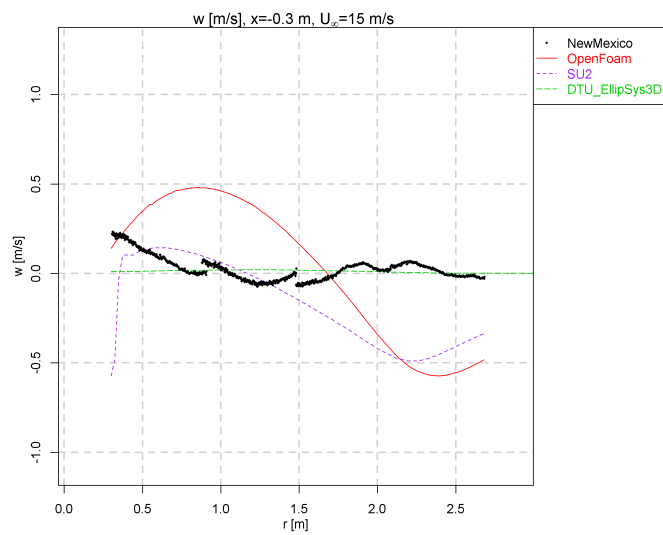
Figure 64: Radial traverse velocity w at axial location x=-0.3m for the freestream velocity of 24m/s
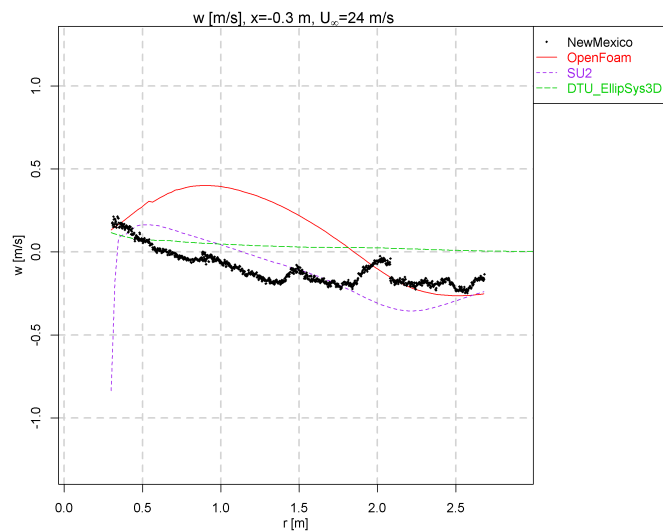
Bibliography

1   K Boorsma and J Schepers. Description of experimental setup new mexico experiment. Technical report, ECN-X–15-093-v3, The Netherlands, 2015.

2   K Boorsma and JG Schepers. Mexnext iii: Definition of first round of calculations. In *Mexnext*, 2017.

3   K Boorsma, JG Schepers, S Gomez-Iradi, I Herraez, T Lutz, P Weihing, L Oggiano, G Pirrung, HA Madsen, WZ Shen, H Rahimi, and P Schaffarczyk. Analysis of mexico wind tunnel measurements: Final report of iea task 29, mexnext (phase 3). (ECN-E–18-003), 2018.

4   Palacios F., Colonno M. R., Aranake A. C., Campos A., Copeland S. R., Economon T. D., Lonkar A. K., Lukaczyk T. W., Taylor T. W. R., and Alonso J. J. Stanford university unstructured (su2): An open-source integrated computational environment for multi-physics simulation and design. *AIAA Paper*, 287:2013, 2013.

5   Weller H. G., Tabor G., Jasak H., and Fureby C. A tensorial approach to computational continuum mechanics using object-oriented techniques. *Computers in physics*, 12(6):620–631, 1998.

6   Jasak H., Jemcov A., and Tukovic Z. Openfoam: A c++ library for complex physics simulations. In *International workshop on coupled methods in numerical dynamics*, volume 1000, pages 1–20. IUC Dubrovnik, Croatia, 2007.